Experimental analysis on CPA-free thin-disk multipass amplifiers operated in a helium-rich atmosphere

FLORIAN BIENERT,[*] **ANDRÉ LOESCHER,** **CHRISTOPH RÖCKER,** **THOMAS GRAF,** **AND MARWAN ABDOU AHMED**

Universität Stuttgart, Institut für Strahlwerkzeuge (IFSW), Pfaffenwaldring 43, 70569 Stuttgart, Germany
[*]*florian.bienert@ifsw.uni-stuttgart.de*

Abstract: We present an experimental investigation on the benefits of helium as an atmospheric gas in CPA-free thin-disk multipass amplifiers (TDMPAs) for the amplification to average powers exceeding 1 kW and pulse peak powers reaching 5 GW. Both the performance of the amplifier and the properties of the amplified sub-400 fs laser pulses centred at a wavelength of 1030 nm are compared for different helium concentrations in air, outlining and quantifying the benefits of a helium-rich atmosphere. The amplification of 100 μJ pulses in an atmosphere with 60% helium instead of air led to a maximum increase in efficiency from 24% to 29%. This translated into an increase of average output power and pulse energy of 34 W (i.e +19%) and 0.34 mJ (i.e. +19%) respectively. At the same time an improvement of the beam quality from $M^2 = 1.18$ to $M^2 = 1.14$ was achieved. For the amplification of 10 μJ pulses to over 1 kW of average power an atmosphere with 33% helium led to an improved beam pointing stability by a factor of 2. Moreover, the beam propagation factor M^2 improved by 0.1, and the power stability improved by approximately 10%.

1. Introduction

The development and concomitant availability of lasers delivering ultra-short pulses with high pulse energies and high average powers have led to a wide variety of applications. Examples in the field of material processing are drilling of deep micro-holes [1–3], cutting of carbon fiber reinforced plastics [4,5], welding of glass [6–8], or surface structuring to create hydrophobic surfaces [9,10]. Besides this, such lasers have also become important for scientific applications such as the creation of attosecond pulse trains by means of high-harmonic generation [11–13], as pump lasers for optical parametric amplifiers [14,15], or even the creation of filaments to trigger lightning [16–18]. While the purposes are very different, all these applications require a high average or high peak power as well as high flexibility in terms of pulse parameters. A reduction of the price of such lasers additionally would increase the impact and dissemination of these technologies in the industry. Thin-disk multipass amplifiers (TDMPA) are suitable systems to meet all the named requirements. Their passive concept enables the amplification of pulses with repetition rates ranging from the Hz [19], over the kHz [20] to the MHz [21] range, and even up to continuous wave (cw) operation [22,23]. This flexibility equally applies to the pulse duration as TDMPAs were demonstrated to support pulses with a duration of several hundred fs [21] as well as pulses with durations in the order of ps- [20], ns- [24], and μs [25]. The amplification of bursts of pulses has also been shown [26]. Compared to other architectures, such as e.g. fibre amplifiers [27], TDMPAs only require chirped-pulse amplification (CPA) at much higher peak intensities in the order of multiple GW/cm^2. This is advantageous, not only in terms of cost but also in terms of reduced complexity. This additionally results in a higher flexibility concerning

the state of polarization (e.g., radial or azimuthal polarization [28,29]) since both the stretchers and the compressors typically used for CPA are only applicable with linearly polarized radiation. The omission of CPA in TDMPAs is possible thanks to the short interaction length and large diameter of the amplified beam inside the laser disk. The large diameter of the beam leads to low peak intensities of the pulses which effectively reduces the nonlinear effects. Despite these advantages, the peak power achieved by CPA-free TDMPAs cannot be scaled arbitrarily. Even with this concept degradations of the optical efficiency, the pulse shape, and the beam quality occur as a consequence of self-focusing at some point and may even lead to damage of optical elements. This was already observed in one of our previous experiments where sub-ps pulses were amplified to 2 GW of peak power which led to strong spectral broadening [20,30].

Although these experiments show the physical limitations set by the nonlinearities, the aim to scale the peak power while maintaining the flexibility and the affordability of a CPA-free amplification scheme is still pursued. The operation of the amplifier system in a helium atmosphere is known to be a promising solution for this purpose. The pulses inside TDMPAs travel in atmospheric gas over the largest part of the propagation distance (> 150 m), which is why its contribution to the resulting nonlinearity is expected to dominate the effects caused within the short path inside the optical elements. As helium exhibits a nonlinear refractive index n_2 which is two orders of magnitude lower than that of air [31,32] it is commonly used in mode-locked oscillators to mitigate nonlinear effects [33,34]. Thanks to its 9-times lower thermal dispersion [35–37] it is also used in cw thin-disk oscillators [38,39] and TDMPAs [21,22] to reduce thermal lensing and the effects of the air wedge, which are both consequences of the heated ambient gas [40].

So far, the benefits of helium were mainly pointed out for thin-disk-based cw-systems or mode-locked oscillators. No comprehensive investigation on the influence of helium in TDMPAs was presented so far, although both the aspects of heated gas and high nonlinearities are combined in these systems due to the presence of both high average and high peak powers. The motivation of this paper is therefore to investigate the influence and benefits of different helium concentrations in the TDMPA's atmosphere both on the performance of the system as well as on the properties of the amplified pulses. Two series of experiments were carried out for this purpose. The first one (presented in section 4) was devoted to the influence of helium on the nonlinear effects. The second series of experiments (presented in section 5) served the investigation of the influence of helium on the stability of the TDMPA when operated at high average powers exceeding 1 kW.

2. Setup

Figure 1 schematically shows the experimental setup, which is based on the TDMPA presented in Ref. [21]. We used a Spirit-100 laser from MKS Spectra Physics as the seed. It delivers pulses with a maximum repetition rate of 1 MHz at an average power of 100 W. The repetition rate and pulse energy can be reduced using its internal acousto-optic modulator (AOM) while maintaining a constant pulse duration of $\tau = 271$ fs (FWHM, sech^2), beam diameter, and beam propagation factor ($M^2_{hor.} = 1.12$, $M^2_{vert.} = 1.1$). The seed beam with a diameter of 4 mm was guided into the TDMPA's box through an anti-reflection (AR) coated fused-silica window. The TDMPA comprises an array of 80 mirrors, which allows for 40 reflections of the amplified beam on the highly-reflective (HR) coated backside of the Yb:YAG thin disk [21,41]. The disk was doped with a concentration of 10-at.% Yb, had a radius of curvature of 20 m and a thickness of approx. 125 μm. The TDMPA is enclosed in a sealed box made of PMMA. The latter has a volume of 0.68 m^3 and an inlet through which the helium (5.0 purity) was delivered. As shown in Fig. 1, the helium concentration was monitored by means of a helium sensor (XP-3140, New Cosmos Electric). Using this mobile sensor, it was found that the helium concentration was distributed homogenously approx. 15 min after closing the inlet. The Yb:YAG thin-disk crystal was pumped by a fiber-coupled spectrally stabilized diode laser from DILAS-Coherent delivering

up to 1.8 kW of power centered at a wavelength of 969 nm with a spectral bandwidth of less than 0.5 nm (FWHM). After the amplification, still inside the box, the beam is directed over a mirror with a reflectivity of 99%, where it is split into the reflected high-intensity (see solid line) main beam and a transmitted low-intensity replica (see dashed line) used for diagnostic purposes. Both beams are then guided out of the box through a laser window. The high-intensity beam is split once more at an additional mirror with a reflectivity of 99% where its reflected and transmitted parts are guided onto the power head and towards the beam analysis, respectively. The approach of generating two low-intensity replicas of the amplified beam, one inside the TDMPA box (dashed line) and one outside (dotted line), allows to investigate the nonlinear effects introduced by the exit window of the TDMPA as explained in the following section.
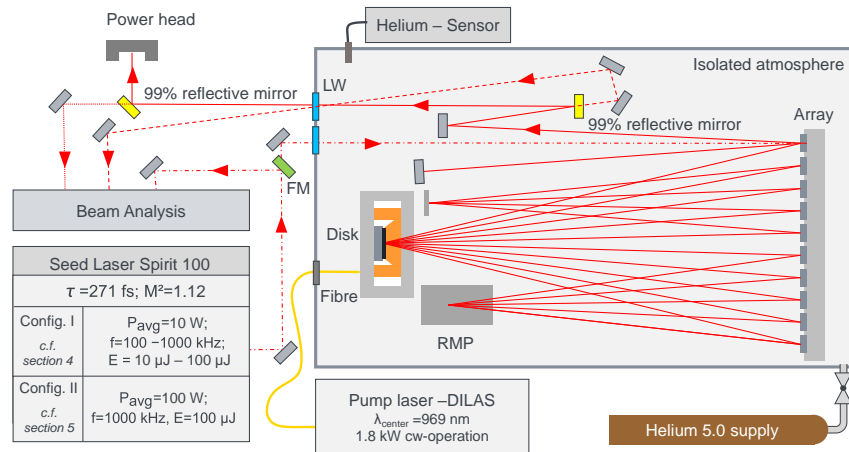
Fig. 1. Experimental setup. The TDMPA is located in a controlled air-helium atmosphere. The dash-dotted and solid lines indicate the paths of the seed and amplified beam, respectively. The dashed and the dotted line indicate the beam path of the low-intensity replica of the amplified beam, which results from the transmission through a mirror with a reflectivity of 99% (shown in yellow). RMP: retro-reflecting mirror pair, LW: Laser window, FM: Flip-mirror.

3. Theoretical analysis of the nonlinearity in the system

The coefficient γ_{SPM} of self-phase modulation (SPM) is a measure for the nonlinearity experienced by a beam along its propagation in a given medium. Assuming a Gaussian beam profile it can be defined as

$$\gamma_{SPM} = \frac{2 \cdot k \cdot n_2}{\pi} \int \frac{1}{w^2(z)} dz, \tag{1}$$

where n_2, w, k and z denote the nonlinear refractive index of the corresponding medium, the beam radius, the propagation constant, and the direction of propagation, respectively [42]. Since the calculation of the B-Integral additionally requires knowledge on the development of the power inside the amplifier, which cannot easily be monitored in our experiments, we have chosen the SPM-coefficient as the main measure to analyze the nonlinearity of the system. The two media mainly contributing to the nonlinearity experienced by the pulses are the Yb:YAG laser crystal and the ambient gas inside the amplifier's housing. The influences of the ambient gas in front of the amplifier's housing and the fused-silica entrance window are neglected since the intensity of the seeded pulses is low. Since the pulses have a high intensity after the amplification, the beam was split into a low-intensity and a high-intensity beam already inside the box, which allowed to investigate and exclude (when analyzing the low-intensity beam) the influence of the

non-linearities in the exit window and the ambient gas outside the amplifier's housing. From the periodic modulation of the beam diameter inside the TDMPA [41], we calculated the contribution of both relevant media (i.e. the laser disk and the ambient gas) using Eq. (1) separately. The total propagation distances in the ambient gas within the TDMPA and the disk were $L_{gas} = 192$ m and $L_{disk} = 10$ mm, respectively. Using the nonlinear refractive indices $n_{2,air} = 2.9 \cdot 10^{-17}$ mm^2/W [31], $n_{2,helium} = 0.04 \cdot 10^{-17}$ mm^2/W [32], and $n_{2,disk} = 6.13 \cdot 10^{-14}$ mm^2/W [43] for air, helium, and YAG, respectively, the SPM coefficients of these media were calculated to be $\gamma_{air} = 2.36$ rad/GW, $\gamma_{he} = 0.036$ rad/GW and $\gamma_{disk} = 0.26$ rad/GW. In order to determine the total SPM coefficient γ_{total} of our system we assumed the SPM coefficient of the atmosphere γ_{atmo} inside the TDMPA to be linearly dependent on the helium concentrations C_{he} as expressed by

$$\gamma_{total} = \gamma_{atmo} + \gamma_{disk} = \gamma_{air} \cdot (1 - C_{he}) + \gamma_{he} \cdot C_{he} + \gamma_{disk}. \quad (2)$$

Figure 2 shows the resulting total SPM-coefficient γ_{total} (solid black) as a function of the helium concentration C_{he}, as well as the contribution of the disk γ_{disk} (which is independent of C_{he}, dotted black) and the ambient atmosphere γ_{atmo} (dash-dotted black) in the box of the TDMPA. It is seen that γ_{total} decreases linearly with increasing C_{he}. The ratio $\gamma_{atmo}/\gamma_{total}$ (red) which is additionally shown in Fig. 2, illustrates the dominant contribution of the atmosphere to the total nonlinearity of the system. It can be concluded that a helium concentration of 90% is required in order to reduce the contribution of the atmosphere to the value of the total SPM-coefficient down to the one of the disk. A change in beam diameter or unintentional thermal lensing in the system has no significant impact on this. Although the total SPM-coefficients would be altered, our calculations showed that, as a consequence of our modulation scheme, the ratio $\gamma_{atmo}/\gamma_{total}$ remains virtually unchanged. In conclusion, this analysis clearly shows that efforts should first be made to reduce the nonlinearity caused by the atmosphere before addressing the nonlinearity caused by the disk.
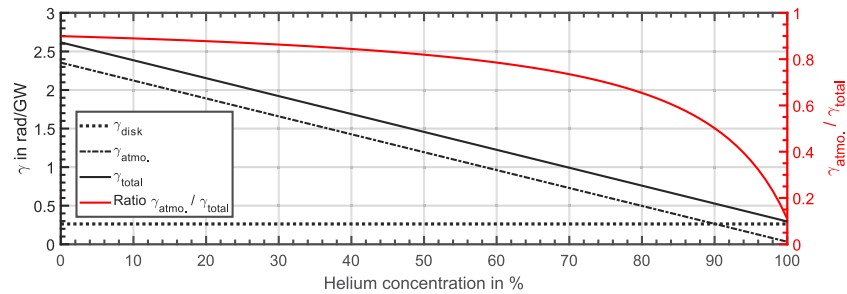
Fig. 2. Calculated SPM-coefficients γ of the disk, the atmosphere inside the TDMPA, and the total system in dependence on the helium concentration. The ratio $\gamma_{atmo}/\gamma_{total}$ illustrates the relative contribution of the atmosphere inside the TDMPA to the nonlinearity of the overall system.

4. Experimental investigation on the nonlinearity of the system

In order to investigate the influence of a helium atmosphere on the nonlinear effects accumulated in the TDMPA, both the helium concentration and the energy (and hence the intensity) of the seed pulses were modified in a series of experiments. At the same time, to allow for comparability of the experiments, the average power of the seeded pulses was set at a constant level which required a variation of the repetition rate of the seed laser. Table 1 gives an overview of the properties of the applied seeded pulses, resulting from this condition.

The amplification of the pulses with the four different seeded pulse energies is carried out for three different gas mixtures inside the amplifier (atmospheres) resulting in the conduction of

Table 1. Parameters of the four different seed laser configurations. The pulse duration was measured to be 271 fs (FWHM, $sech^2$) in all cases.

Repetition rate [kHz]	100	200	500	1000
Average power [W]	10	10	10	10
Pulse energy [µJ]	100	50	20	10
Peak power [MW]	325	162	65	32.5

12 different experiments. For the first atmosphere, which served as a reference, we used air at atmospheric pressure and humidity of approx. 30%. In the following, we will refer to it as a concentration of 0% helium. The other two atmospheres are helium-air mixtures at atmospheric pressure with a helium concentration of 33% and 60%. Because of our current sealing of the system and since we wanted to ensure a constant helium concentration (±3% due to volatilization) over the full time of the experiments, we did not attempt to perform experiments with higher helium concentrations. The measurement of the spectra, the beam quality, and the pulse duration presented in the following were all performed on the low-intensity replica separated from the beam already inside the TDMPA-box (dashed line in Fig. 1) to exclude the influence of nonlinearities induced by the exit window and the atmosphere outside of the amplifier.

4.1. Extraction efficiency
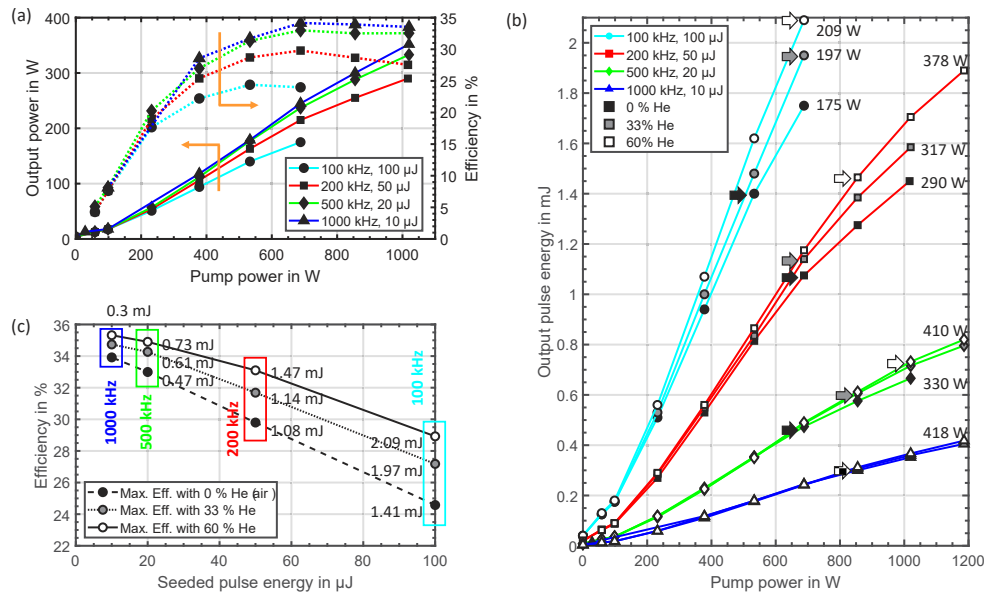
Fig. 3. (a): Output power and amplification efficiency measured with different energies of the seeded pulses for the operation in air. (b): Pulse energy measured for different energies of the seeded pulses in different atmospheres. The labels indicate the reached average output power at the upper end of each curve. The arrows indicate the points where maximum efficiency was achieved. (c): Maximum achieved efficiency for different energies of the seeded pulses and different atmospheres. The labels indicate the output pulse energy achieved at the point with maximum extraction efficiency. The corresponding pump powers can be read from fig (b).

Figure 3(a) shows the average output power and the extraction efficiency of the amplified pulses for the four different seeded pulse energies for the operation in air (0% of helium). The extraction efficiency is calculated as $(P_{out} - P_{seed})/P_{pump}$. The results show that both the output power and the efficiency were significantly reduced when seed pulses with higher energies, i.e. higher intensities, were launched into the TDMPA. This reduction is stronger at higher pulse energies, as can be seen by comparing the efficiency of the experiments with seeded pulse energies of 100 µJ and 50 µJ to the ones with 20 µJ and 10 µJ. We attribute this behavior to spectral broadening induced by SPM as a consequence of the increased intensity of the propagating laser pulses. This spectral broadening leads to a reduction of the spectral overlap of the gain and the laser pulses.

This hypothesis is supported by the observed influence of an increasing helium concentration on the achieved output pulse energy shown in Fig. 3(b) which comprises the results achieved with all 12 combinations of atmosphere and seeded pulse energies. For all energies of the seeded pulses and at all pump power levels, an increase of the helium concentration led to an increased energy of the amplified pulses which corresponds to a higher extraction efficiency. The data for the 0% He-concentration shown in Fig. 3(b) corresponds to the one in Fig. 3(a). Figure 3(c) shows the maximum achieved extraction efficiencies for each of the 12 different experiments as a function of the seeded pulse energy. The data points correspond to the ones highlighted by the arrows in Fig. 3(b). The data shows a clear decrease in extraction efficiency with increasing pulse energy, i.e. increasing intensities of the seeded pulses. This decrease is however reduced when the helium concentration is increased. The proof that this is caused by the changing spectral overlap of the gain and the pulses as a consequence of spectral broadening can be found with the analysis of the measured spectra presented in the following section.

4.2. Spectra of the extracted pulses

Figures 4 and 5 show the evolution of the spectral intensity distribution of the laser pulses exiting the amplifier in dependence on their pulse energy.

The spectral measurements were performed on the replica that was created inside the box, cf. dashed line in Fig. 1. To enable a quantitative comparison of the spectra, we used the first and the second moment of the distribution as a measure for the center of gravity and the width of the spectrum, respectively. These quantities were chosen since the location of the peak, as indicated by the black line, and the full width at half maximum (FWHM, not shown) were found to be unsuitable measures due to the complex spectral intensity distributions. The green lines in Fig. 4 connect the locations where 5% of the peak intensity is reached in the spectra. This additional measure was added to highlight the effect of spectral broadening as it includes low-intensity parts of the spectrum which cannot yet be considered as noise. To facilitate the comparison, the spectra of the seeded laser pulses are shown (cyan-colored) on the bottom line of each figure. The redshift of the pulses when propagated through the un-pumped TDPMA (pump power 0 W) originates from the stronger absorption of the shorter wavelengths (with respect to the central wavelength of 1030 nm) in the un-pumped Yb:YAG disk as described by Koerner et. al [44].

When analyzing the spectral evolution of the pulses amplified in air with 0% of helium for a seeded pulse energy of 100 µJ, SPM-induced spectral broadening is already noticeable when comparing the spectra of the seeded laser pulses and the one of the output pulses with the unpumped MPA, i.e. the "amplified" pulse at 0 W of pump power. For the seed pulses with 100 µJ, this spectral broadening increases significantly with increasing pump power of the MPA as the energy of the amplified pulses increases correspondingly. This behavior can also be observed for the seed pulses with 50 µJ of energy, albeit with a slight shift to higher pump powers, respectively amplified pulse energies. The spectra of the seeded pulses with 20 µJ and 10 µJ of energy (see Fig. 5) on the other hand exhibit only little or no spectral broadening. For seeded pulses with an energy of 10 µJ, the beneficial use of helium can however still be observed when comparing the
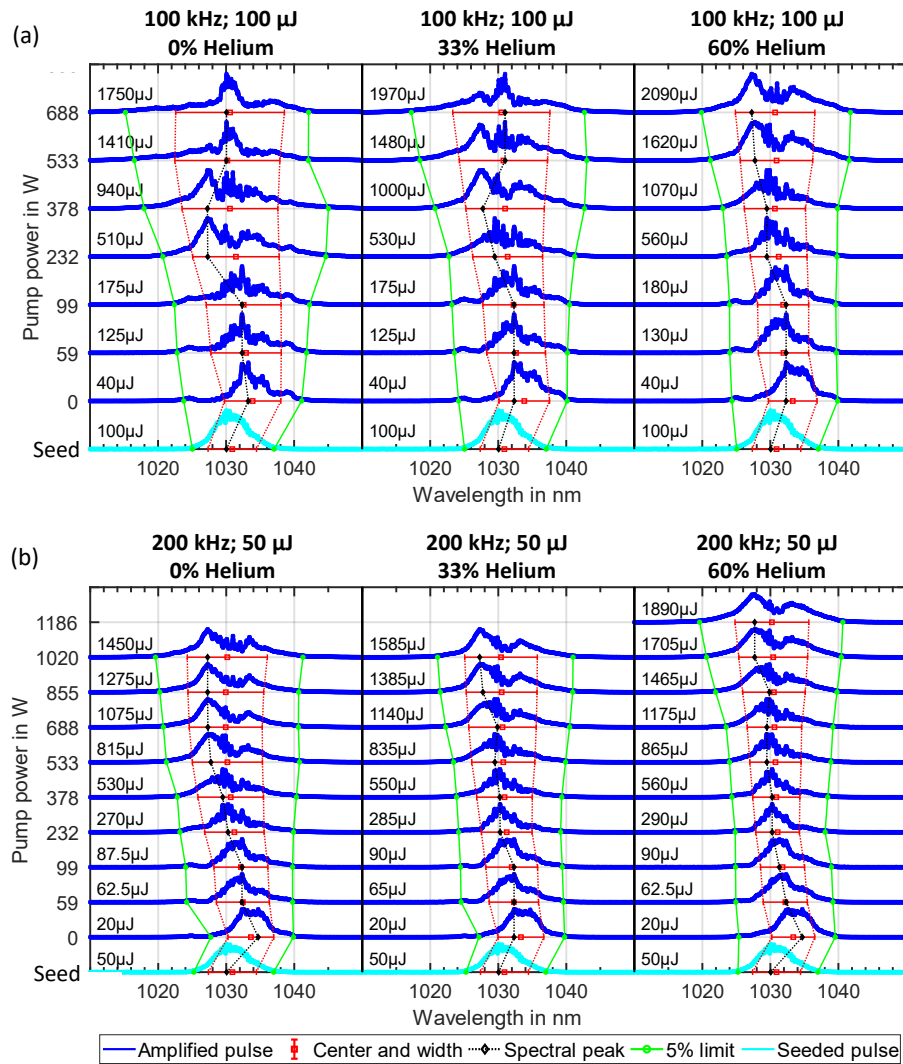
Fig. 4. Normalized spectral intensity of the amplified laser pulses (blue) and of the seeded pulses (cyan) for seeded pulse energies of 100 µJ (a) and 50 µJ (b) in dependence of the pump power at helium concentrations of 0% (left), 33% (middle), and 60% (right). The centre of gravity (red dots) and the width of the spectra (red error bars) were calculated by means of the first and second moment of the distribution, respectively. The pulse energy is indicated at the corresponding pump power level.
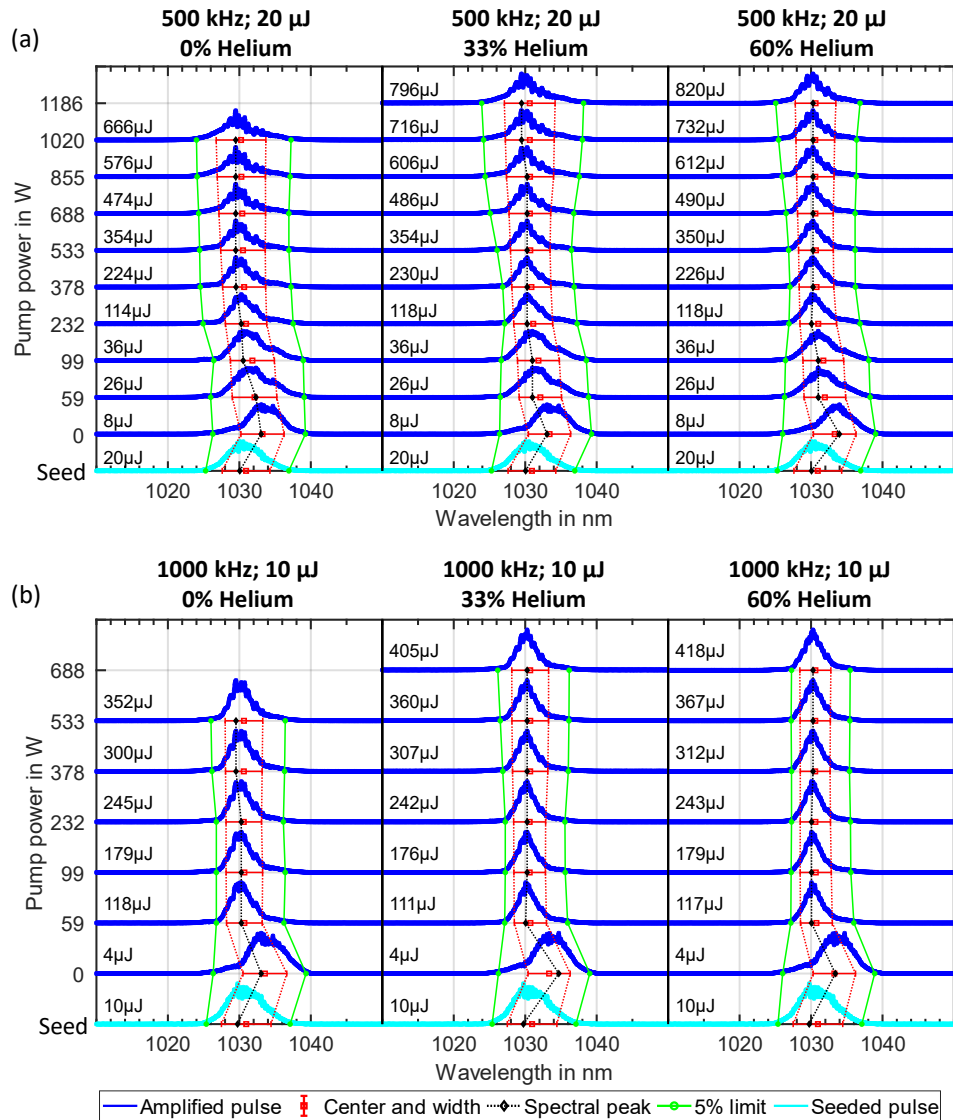
Fig. 5. Normalized spectral intensity of the amplified laser pulses (blue) and of the seeded pulses (cyan) for seeded pulse energies of 20 µJ (a) and 10 µJ (b) in dependence of the pump power at helium concentrations of 0% (left), 33% (middle), and 60% (right). The centre of gravity (red dots) and the width of the spectra (red error bars) were calculated by means of the first and second moment of the distribution, respectively. The pulse energy is indicated at the corresponding pump power level.

spectra of the pulses amplified in an atmosphere with 0% of helium to the ones amplified in 60% of helium.

Although the pulses were amplified to different pulse energies and in different atmospheres, their spectra show high similarities. They seem to go through a similar evolution with increasing pump power and hence increasing pulse energy. First, the spectrum becomes homogeneously broadened (see Fig. 4(a), 0% He, pump power: 99 W). Second, the spectrum forms a double peak with a predominant part on the blue side of the spectrum (see Fig. 4(a), 0% He, pump

power: 232 W) and finally, a peak at 1030 nm on a broad pedestal is formed, (see Fig. 4(a), 0% He, pump power: 533 W). This evolution can be shifted to higher pulse energies either by using a higher helium concentration (see Fig. 4(a), 60% helium) or by decreasing the seeded pulse energy (see Fig. 4(b), 0% He).

A quantitative comparison of the presented spectra is shown in Fig. 6(a) and 6(b), where the spectral bandwidth (given by the second moment) is shown as a function of the achieved output power, and pulse energy, respectively. To facilitate the comparison in terms of efficiency, light-grey lines connect points with identical pump power in Fig. 6(a). Both figures show that the spectral bandwidth increases with increasing energy for the seeded pulses with 100 µJ and 50 µJ of energy as already indicated by the spectra shown in Fig. 4. This spectral broadening is reduced with increasing helium concentrations and even leads to a decrease of the spectral bandwidth of the output pulses with respect to the one of the seeded pulses with low energy. This behavior, especially pronounced for the seed pulses with an energy 10 µJ was also already indicated by the spectra, cf. Figure 5(b) and is attributed to gain narrowing.
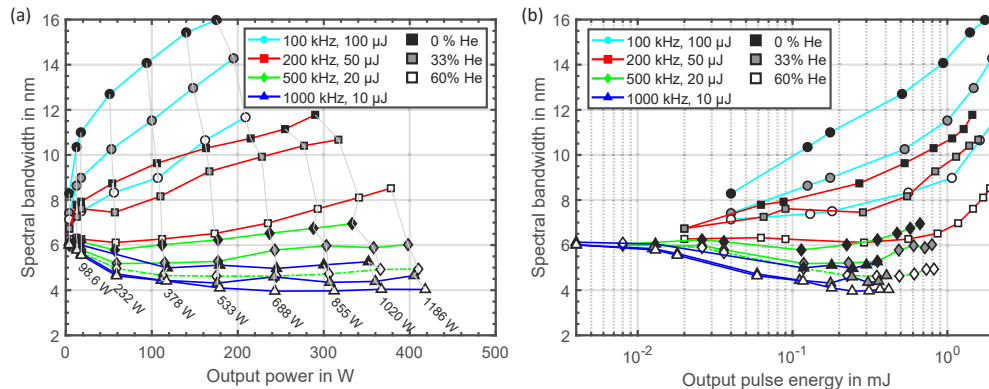

Fig. 6. (a): Spectral bandwidth of the amplified laser pulses for different energies of the seeded pulses and different helium concentrations as a function of the achieved output power. The grey lines connect points with identical pump power as specified by the tags at the lowest curves in the graphs. (b): Spectral bandwidth of the amplified laser pulses for different energies of the seeded pulses and different helium concentrations as a function of the achieved output pulse energy.

Figure 6(a) also shows that the output power is reduced at constant pump power (see gray lines) when the spectral bandwidth is increased. This supports the conclusion drawn from the results depicted in Fig. 3 where the decreased efficiency was attributed to the reduced overlap of the spectral gain and the broadened spectral intensity of the laser pulses. Comparable observation could also be drawn when using by the 5%-limit instead of the second moment.

4.3. Duration and peak power of the extracted pulses

Since the helium concentration had a strong influence on the spectrum of the amplified pulses it is expected to also affect the pulse duration. The latter was measured with an autocorrelator (APE PulseCheck) using the low-energy replica of the pulses created inside the box, cf. dashed line in Fig. 1, and where it was found that the pulse shape followed a sech^2 function with high accuracy for almost all measurements. Exceptions from this sech^2 shape, showing slight formation of wings, were only observed at the maximum power for the pulses with a seeded energy of 100 µJ (100 kHz) and a helium concentration of 0% leading to an output energy of 1.75 mJ. Figure 7(a) shows the measured durations of the amplified pulses as a function of the pulse energy. The measurements manifest an increase of the pulse duration at first, followed by a

subsequent decrease. The exact details of this interplay could not be determined using the present measurements as it would require additional information on the pulses' spectral and temporal phase not only after the amplification but also after each of the passes through the laser disk. In Fig. 7(b) the peak power of the output pulses is plotted against the output power. The highest achieved pulse peak power was 5 GW, reached for a seeded pulse energy of 100 µJ (100 kHz) at a helium concentration of 33%.
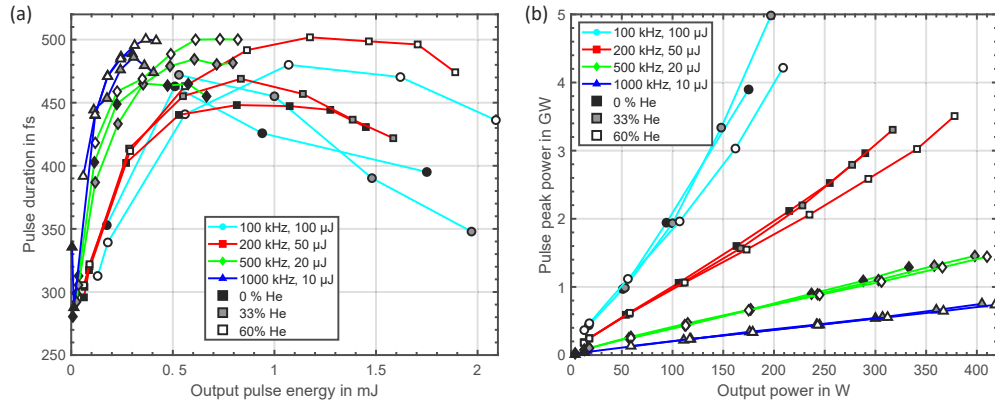
Fig. 7. Duration of the amplified pulses as a function of the output pulse energy (a) and peak power of the amplified pulses as a function of the output power (b) for the different seeded pulse energies and helium concentrations.

Both the pulse duration and the corresponding pulse peak power show that a high helium concentration is not a guarantee for high peak powers. Although it helps to increase the pulse energy, as shown in section 4.1, it does not assure a short pulse duration. The pulse duration depends on many factors such as the properties of the incident pulses, the system's dispersion, the gain narrowing arising in the disk and spectral broadening. Since all of these factors are coupled and since they influence each other during the whole amplification process, the influence of helium on the pulse duration and thus on the peak power cannot be generalized.

4.4. Beam propagation factor M^2

Figure 8(a) summarizes the measurements of the beam propagation factor M^2 of the amplified beam (measured on the low-energy replica separated from the main beam inside the box, cf. dashed line in Fig. 1) as a function of the output pulse energy. While at first all curves show a decreasing M^2-value with increasing output pulse energy, a subsequent increase starting around 0.5 mJ to 1 mJ of output energy is observed with the seeded pulse energies of 100 µJ and 50 µJ. This deterioration of the beam quality at high output energy is however significantly reduced with higher helium concentration. With the lower seeded pulse energies of 20 µJ and 10 µJ the M^2-value is diminishing with increasing output pulse energy almost until the maximum output energy is reached and no significant influence of the helium concentration is observed.

Figure 8(b) shows the beam propagation factors measured when the amplifier was operated at the point providing the maximum extraction efficiency, cf. Figure 3. It is observed that the beam quality of the amplified beam degrades with increasing pulse energies i.e., higher intensities of the seeded pulses and that an increasing helium concentration leads to improved beam quality, as already indicated in Fig. 8(a).

The deterioration of the beam quality generally originates from a modification of the laser beam's phase or intensity. When a phase term added to the beam is not constant nor linear nor quadratic it generally degrades the beam quality [45,46]. For the degradation of the beam
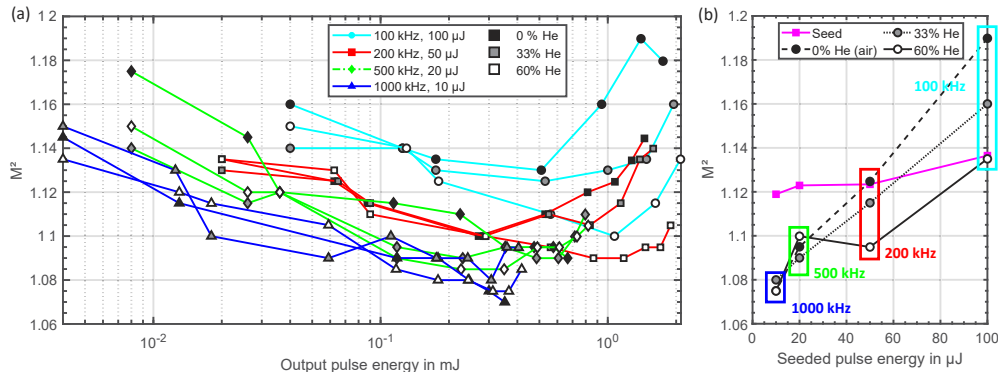
Fig. 8. (a): Beam propagation factor M^2 as a function of the achieved output pulse energy. (b): Beam propagation factor M^2 obtained at the point with the maximum efficiency as a function of the seeded pulse energy. The beam propagation factor M^2 of the seed laser is shown for reference.

quality of the pulses with the higher seed pulse energies (100 µJ and 50 µJ), possible intrinsic or thermally introduced deformations of the optics can be excluded since the pulses with the low seeded pulse energy of 10 µJ pass the same optics as the pulses of the other configurations, but show excellent beam quality although they were amplified to even higher average output powers. Using the same reasoning, it can also be ruled out that the higher thermal dispersion of air amounting to dn/dT $\approx -9 \cdot 10^{-7}$ [35,37] degrades the beam quality; helium has a dn/dT $\approx -1 \cdot 10^{-7}$ [36] at ambient pressure for a wavelength around 1 µm. We hence conclude that the nonlinearities, i.e. the spatial Kerr-effect lead to an increase of the M^2-value. It causes a phase distribution that follows the intensity profile (i.e. approximately Gaussian) and therefore introduces higher-order phase distortions [47–49].

5. Long-term stability

In the experiments presented so far, no pronounced instabilities of pointing, power and beam quality were observed with the applied pulse energies and helium concentrations. Since these kinds of instabilities are usually induced by thermal effects, further experiments were carried out with significantly higher average power by increasing the average power of the seed to 100 W with pulses of 100 µJ of energy at a repetition rate of 1000 kHz, see configuration II in Fig. 1. Two experiments were carried out, one in air (0% of helium) and one with a helium-air mixture with 33% helium. The lower helium concentration of 33% rather than 60% was chosen to reduce the influence of losses of the helium (~2% per hour) during the long-term measurements of several hours. An output power exceeding 1 kW was reached at pump power of 1.7 kW both in air with 0% of helium and with 33% of helium. This introduced a sufficient thermal load to the system to investigate the influence of the helium. The measurements presented in the following were taken on the replica separated outside the box (dotted line in Fig. 1).

5.1. Beam pointing stability

Figure 9 summarizes the stability of the beam pointing (a to d) for the operation of the amplifier in air (left column) and with 33% of helium (right column). The measurement of the pointing was recorded with a detector system from TEM Messtechnik GmbH, which was placed in the beam at a position located approximately 4 m from the amplifier's exit window and operated with a sampling rate of 1 Hz. The system consists of two positional sensitive detectors where one of them is placed at the focus of a lens, thus allowing for the recording of both the beam's angular

and positional fluctuations. The measurements were started after a thermalization time of one hour in order to avoid the influence of the thermal drifts that occur immediately after turning on the system. It is also worth mentioning that no helium was injected during laser operation as this showed to lead to strong pointing fluctuations.
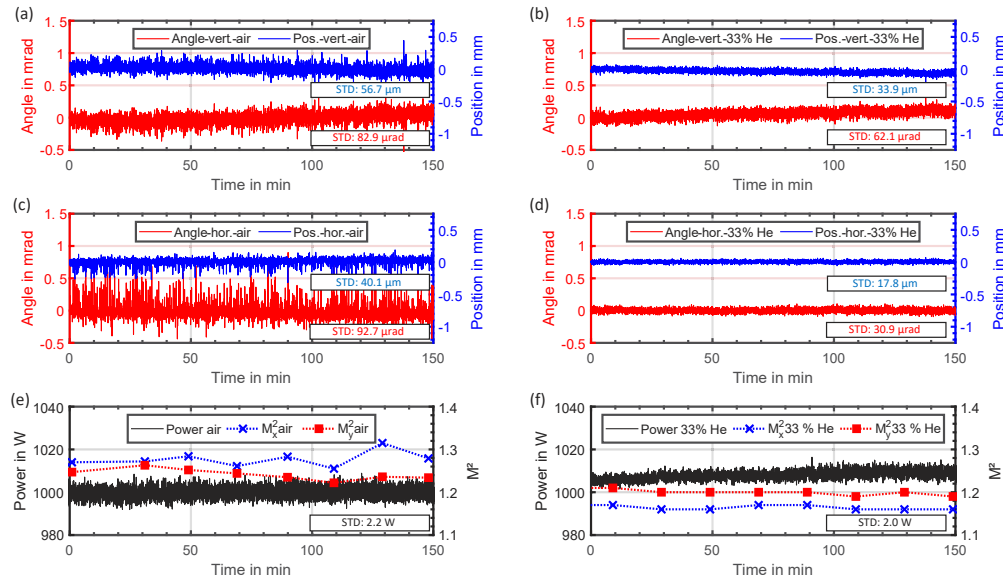
Fig. 9. Angular and positional pointing in the vertical (top row) and horizontal (middle row) direction for operation in air (left column) and with 33% of helium (right column). Output power and beam propagation factor M^2 for the operation of the system in air (e) and with 33% of helium (f).

The comparison of the results shows that the fluctuations are reduced by a factor of approximately two when operating the system in an atmosphere with a helium concentration of 33%. Although helium and air have different heat capacities and different thermal conductivities, no significant difference of the temperatures of the atmospheres and the various components of the TDMPA were observed. The fact that operation in air nevertheless results in much stronger pointing fluctuations is mainly attributed to stronger thermally induced gas lenses and wedges [22,38,39] due to the higher thermal dispersion dn/dT of air as compared to the one of the helium-air mixture.

5.2. *Power stability*

The black curves in Fig. 9(e) and 9(f) show the output power of the system recorded at a sampling rate of 2 Hz when the amplifier was operated in air and the air-helium mixture, respectively. The comparison shows that the output power is higher when the amplifier is operated in the atmosphere with 33% of helium. The reason for this is the reduced spectral broadening and the therefore increased overlap of the gain spectrum and the spectrum of the laser pulses discussed above. The larger power fluctuations in air however originate from the larger pointing fluctuations of the beam since the output power strongly depends on the spatial overlap of the beams with the pump spot on the laser disk.

5.3. Stability of the beam propagation factor M^2

The red and blue data points in Fig. 9(e) and 9(f) show the measured beam propagation factor M^2 of the amplified beam. The comparison shows an overall improved M^2 by approximately 0.1 when operating the system in an atmosphere with 33% of helium instead of air, which is attributed both to the helium's lower nonlinear refractive index n_2 and its lower thermal dispersion dn/dT. The stronger fluctuations of the value of the M^2 when the TDMPA is operated in air may also be attributed to the pointing fluctuation of the beam mentioned above.

6. Discussion

A high helium concentration in the amplifier's atmosphere showed to be beneficial both with respect to the achievable pulse energies, average power and temporal stability. This raises the question of the extent to which the advantages of helium could be further exploited, i.e. what could be achieved by further increasing the helium concentration. A hint on this is given in Fig. 10. Here the maximum achieved efficiencies of the amplifier operated with the different seeded energies mentioned in Table 1 are displayed as a function of the measured helium concentration. The linear extrapolation shows what maximum efficiency can be expected when the TDMPA would be operated in a pure helium atmosphere.
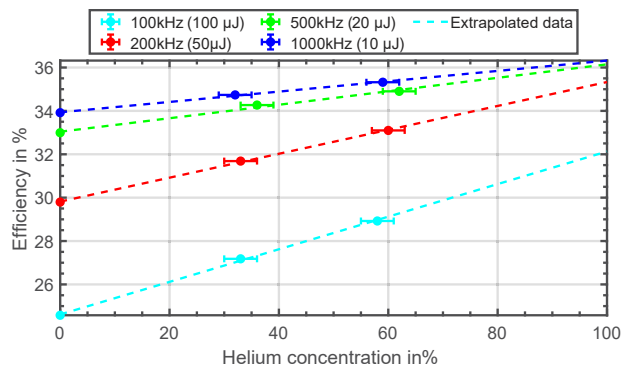
Fig. 10. Maximum measured efficiencies obtained with the different seeded pulse energies as a function of the measured helium concentration. The dashed lines represent linear extrapolations.

The extrapolations indicate that there is still some potential to improve the performance of the system by increasing the helium concentration (thus mitigating the nonlinear effects) especially in the case of the higher seeded pulse energies. However, even in a pure helium atmosphere the influence of the nonlinear effects cannot be avoided completely as seen by the difference of the expected efficiencies at 100% of helium for the different seeded pulse energies since the nonlinearities of the optical components and especially the one of the laser disk are not affected by varying the atmosphere.

7. Conclusion and outlook

In conclusion our investigations showed that helium, used as atmospheric gas, improved the performance of our TDMPA. As a consequence of the lower non-linear refractive index of helium, the amplified pulses experienced lower spectral broadening and showed improvements in terms of output power i.e., pulse energy, efficiency, and beam quality. It was additionally demonstrated that the improvements are more significant the higher the helium concentration and the larger the seeded pulse energy. For the seed pulses with the highest energy (100 µJ) and at maximum pump

power (688 W) the atmosphere with 33% helium enabled an efficiency increase from 24% (air) to 27% and up to 29% for an atmosphere with 60% helium. This corresponds to an improvement of output power and pulse energy by 20 W and 0.2 mJ (11%) and 34 W and 0.34 mJ (19%) for the 33% and 60% helium concentrations. At the same time, the beam propagation factor was reduced from $M^2 = 1.18$ (air) to $M^2 = 1.16$ (33% helium) and $M^2 = 1.14$ (60% helium). Moreover, for the pulses with the second highest seed energy, the improvements were significant, i.e., an increase in efficiency from 27.5% (air) to 30.1% and 32.5% for the two helium concentrations and at maximum pump power. For the two other seed configurations with lower pulse energy the improvements were less significant but still observable. When amplifying to higher average powers, exceeding 1 kW, the lower thermal dispersion of helium becomes effective as well, which had a beneficial influence on the system's stability. At a helium concentration of 33%, a reduction of the pointing fluctuations by a factor of around 2 was reached together with an improvement of output power stability of 10%. Moreover, the time-dependent fluctuations of the beam quality were drastically reduced by a factor of 2 while the overall beam propagation factor M^2 was improved by approximately 0.1. In the future, we plan to scale the system's pulse energy exceeding 10 mJ with average powers over 1 kW. Furthermore, we plan to implement a flexible seed allowing for the tuning of the repetition rate up to 22 GHz and burst-mode operation with adaptable inter- and intra-burst repetition rates.

Disclosures. The authors declare no conflict of interest

Data availability. Data underlying the results presented in this paper are not publicly available at this time but may be obtained from the authors upon reasonable request.

References

1. D. J. Förster, R. Weber, D. Holder, and T. Graf, "Estimation of the depth limit for percussion drilling with picosecond laser pulses," Opt. Express **26**(9), 11546–11552 (2018).
2. H. Huang, L.-M. Yang, and J. Liu, "Micro-hole drilling and cutting using femtosecond fiber laser," Opt. Eng. **53**, 1–9 (2014).
3. M. Henn, G. Reichardt, R. Weber, T. Graf, and M. Liewald, "Dry Metal Forming Using Volatile Lubricants Injected into the Forming Tool Through Flow-Optimized, Laser-Drilled Microholes," JOM **72**(7), 2517–2524 (2020).
4. R. Weber, C. Freitag, T. V. Kononenko, M. Hafner, V. Onuseit, P. Berger, and T. Graf, "Short-pulse Laser Processing of CFRP," Phys. Procedia **39**, 137–146 (2012).
5. K. Takahashi, M. Tsukamoto, S. Masuno, and Y. Sato, "Heat conduction analysis of laser CFRP processing with IR and UV laser light," Compos. Part A Appl. Sci. Manuf. **84**, 114–122 (2016).
6. X. Zhao and Y. C. Shin, "Femtosecond laser drilling of high-aspect ratio microchannels in glass," Appl. Phys. A Mater. Sci. Process. **104**(2), 713–719 (2011).
7. K. Cvecek, S. Dehmel, I. Miyamoto, and M. Schmidt, "A review on glass welding by ultra-short laser pulses," Int. J. Extrem. Manuf. **1**(4), 042001 (2019).
8. D. J. Hwang, T. Y. Choi, and C. P. Grigoropoulos, "Liquid-assisted femtosecond laser drilling of straight and three-dimensional microchannels in glass," Appl. Phys. A Mater. Sci. Process. **79**(3), 605–612 (2004).
9. S. Faas, U. Bielke, R. Weber, and T. Graf, "Scaling the productivity of laser structuring processes using picosecond laser pulses at average powers of up to 420 W to produce superhydrophobic surfaces on stainless steel AISI 316L," Sci. Rep. **9**(1), 1933 (2019).
10. D. Conrad and L. Richter, "Ultra-short pulse laser structuring of molding tools," Phys. Procedia **56**, 1041–1046 (2014).
11. T. T. Luu, V. Scagnoli, S. Saha, L. J. Heyderman, and H. J. Wörner, "Generation of coherent extreme ultraviolet radiation from α–quartz using 50 fs laser pulses at a 1030 nm wavelength and high repetition rates," Opt. Lett. **43**(8), 1790–1793 (2018).
12. M. Osolodkov, F. J. Furch, F. Schell, P. Šušnjar, F. Cavalcante, C. S. Menoni, C. P. Schulz, T. Witting, and M. J. J. Vrakking, "Generation and characterisation of few-pulse attosecond pulse trains at 100 kHz repetition rate," J. Phys. B At. Mol. Opt. Phys. **53**(19), 194003 (2020).
13. P. Ye, T. Csizmadia, L. G. Oldal, H. N. Gopalakrishna, M. Füle, Z. Filus, B. Nagyillés, Z. Divéki, T. Grósz, M. Dumergue, P. Jójárt, I. Seres, Z. Bengery, V. Zuba, Z. Várallyay, B. Major, F. Frassetto, M. Devetta, G. D. Lucarelli, M. Lucchini, B. Moio, S. Stagira, C. Vozzi, L. Poletto, M. Nisoli, D. Charalambidis, S. Kahaly, A. Zaïr, and K. Varjú,

"Attosecond pulse generation at ELI-ALPS 100 kHz repetition rate beamline," J. Phys. B At. Mol. Opt. Phys. **53**, 1–11 (2020).

14. V. Kozich, A. Moguilevski, and K. Heyne, "High energy femtosecond OPA pumped by 1030 nm Yb:KGW laser," Opt. Commun. **285**(21-22), 4515–4518 (2012).

15. G. Andriukaitis, T. Balčiūnas, S. Ališauskas, A. Pugžlys, A. Baltuška, T. Popmintchev, M.-C. Chen, M. M. Murnane, and H. C. Kapteyn, "90 GW peak power few-cycle mid-infrared pulses from an optical parametric amplifier," Opt. Lett. **36**(15), 2755–2757 (2011).

16. J. Kasparian, R. Ackermann, Y.-B. André, G. Méchain, G. Méjean, B. Prade, P. Rohwetter, E. Salmon, K. Stelmaszczyk, J. Yu, A. Mysyrowicz, R. Sauerbrey, L. Woeste, and J.-P. Wolf, "Electric events synchronized with laser filaments in thunderclouds," Opt. Express **16**(8), 5757–5763 (2008).

17. L. De La Cruz, E. Schubert, D. Mongin, S. Klingebiel, M. Schultze, T. Metzger, K. Michel, J. Kasparian, and J.-P. P. Wolf, "High repetition rate ultrashort laser cuts a path through fog," Appl. Phys. Lett. **109**(25), 251105–251105–4 (2016).

18. C. Herkommer, P. Krötz, R. Jung, S. Klingebiel, C. Wandt, R. Bessing, P. Walch, T. Produit, K. Michel, D. Bauer, R. Kienberger, and T. Metzger, "Ultrafast thin-disk multipass amplifier with 720 mJ operating at kilohertz repetition rate for applications in atmospheric research," Opt. Express **28**(20), 30164–30173 (2020).

19. J. Tümmler, R. Jung, H. Stiel, P. V. Nickles, and W. Sandner, "High-repetition-rate chirped-pulse-amplification thin-disk laser system with joule-level pulse energy," Opt. Lett. **34**(9), 1378–1380 (2009).

20. J. P. Negel, A. Loescher, B. Dannecker, P. Oldorf, S. Reichel, R. Peters, M. Abdou Ahmed, and T. Graf, "Thin-disk multipass amplifier for fs pulses delivering 400 W of average and 2.0 GW of peak power for linear polarization as well as 235 W and 1.2 GW for radial polarization," Appl. Phys. B Lasers Opt. **123**(5), 156 (2017).

21. A. Loescher, F. Bienert, C. Röcker, T. Graf, M. Gorjan, J. Aus der Au, and M. Abdou Ahmed, "Thin-disk multipass amplifier delivering sub-400 fs pulses with excellent beam quality at an average power of 1 kW," Opt. Contin. **1**(4), 747–758 (2022).

22. S. Nagel, B. Metzger, D. Bauer, J. Dominik, T. Gottwald, V. Kuhn, A. Killi, T. Dekorsy, and S.-S. Schad, "Thin-disk laser system operating above 10 kW at near fundamental mode beam quality," Opt. Lett. **46**(5), 965–968 (2021).

23. C. Y. Teisset, C. Wandt, M. Schultze, S. Klingebiel, M. Häfner, S. Stark, C. Grebing, J. Negel, H. Höck, M. Scharun, D. Bauer, A. Budnicki, C. Stolzenburg, D. Sutter, A. Killi, T. Metzger, S. Prinz, S. Stark, C. Grebing, J. Negel, H. Höck, M. Scharun, T. Dietz, D. Bauer, A. Budnicki, C. Stolzenburg, D. Sutter, A. Killi, and T. Metzger, "Multi-kW Thin-Disk Amplifiers," in *High-Brightness Sources and Light-Driven Interactions* (Optica Publishing Group, 2018), Vol. 2018, pp. 1–2.

24. A. Antognini, K. Schuhmann, F. D. Amaro, F. Biraben, A. Dax, A. Giesen, T. Graf, T. W. Hänsch, P. Indelicato, L. Julien, C. Y. Kao, P. E. Knowles, F. Kottmann, Y. W. Liu, L. Ludhova, N. Moschüring, F. Mulhauser, T. Nebel, F. Nez, P. Rabinowitz, C. Schwob, D. Taqqu, and R. Pohl, "Thin-disk Yb:YAG oscillator-amplifier laser, ASE and effective Yb: YAG lifetime," IEEE J. Quantum Electron. **45**(8), 993–1005 (2009).

25. M. Siebold, M. Hornung, R. Bödefeld, M. Wolf, J. Koerner, S. Podleska, S. Klingebiel, C. Wandt, F. Krausz, S. Karsch, R. Uecker, J. Hein, and M. C. Kaluza, "High-energy, diode-pumped laser amplification in Yb: CaF2 and Yb: SrF2," Opt. InfoBase Conf. Pap. 28–30 (2009).

26. C. Röcker, A. Loescher, J.-P. P. Negel, M. Delaigue, F. Morin, C. Hönninger, E. Mottay, P. Villeval, A. Holvoet, D. Lupinski, T. Graf, and M. Abdou Ahmed, "Direct amplification of sub-300 fs pulses in a versatile thin-disk multipass amplifier," Opt. Commun. **460**, 125159 (2020).

27. M. Müller, C. Aleshire, A. Klenke, E. Haddad, F. Légaré, A. Tünnermann, and J. Limpert, "10.4 kW coherently combined ultrafast fiber laser," Opt. Lett. **45**(11), 3083–3086 (2020).

28. A. Loescher, J. P. Negel, T. Graf, W. Pallmann, B. Resan, I. Martial, J. Didierjean, F. Lesparre, J. T. Gomes, X. Délen, F. Druon, F. Balembois, P. Georges, and M. Abdou Ahmed, "A 265W and 782 fs amplified radially polarized beam emitted by a thin-disk multipass amplifier," Adv. Solid State Lasers, ASSL **2015**, 4–6 (2015).

29. A. Loescher, C. Röcker, T. Graf, and M. Abdou Ahmed, "Azimuthally polarized picosecond vector beam with 1.7 kW of average output power," Opt. Lett. **46**(14), 3492–3495 (2021).

30. B. Dannecker, J. P. Negel, A. Loescher, P. Oldorf, S. Reichel, R. Peters, T. Graf, and M. Abdou Ahmed, "Exploiting nonlinear spectral broadening in a 400 W Yb:YAG thin-disk multipass amplifier to achieve 2 mJ pulses with sub-150 fs duration," Opt. Commun. **429**, 180–188 (2018).

31. E. T. J. Nibbering, G. Grillon, M. A. Franco, B. S. Prade, and A. Mysyrowicz, "Determination of the inertial contribution to the nonlinear refractive index of air, N_2, and O_2 by use of unfocused high-intensity femtosecond laser pulses," J. Opt. Soc. Am. B **14**(3), 650–660 (1997).

32. C. Brée, A. Demircan, and G. Steinmeyer, "Method for computing the nonlinear refractive index via Keldysh theory," IEEE J. Quantum Electron. **46**(4), 433–437 (2010).

33. T. Südmeyer, S. V. Marchese, C. R. E. Baer, S. Hashimoto, A. G. Engqvist, M. Golling, D. J. H. C. Maas, and U. Keller, "Femtosecond thin disk laser oscillator with pulse energy beyond the 10-microjoule level," Opt. InfoBase Conf. Pap. **16**, 6397–6407 (2008).

34. S. V. Marchese, T. Südmeyer, M. Golling, R. Grange, and U. Keller, "Pulse energy scaling to 5 μJ from a femtosecond thin disk laser," Opt. Lett. **31**(18), 2728–2730 (2006).

35. J. A. Stone and J. H. Zimmerman, "Index of refraction of air," https://emtoolbox.nist.gov/Wavelength/Documentation.asp.

36. J. A. Stone and A. Stejskal, "Using helium as a standard of refractive index: Correcting errors in a gas refractometer," Metrologia **41**(3), 189–197 (2004).

37. R. Penndorf, "Tables of the Refractive Index for Standard Air and the Rayleigh Scattering Coefficient for the Spectral Region between 0.2 and 20.0 µ and Their Application to Atmospheric Optics," J. Opt. Soc. Am. **47**(2), 176–182 (1957).

38. B. Weichelt, D. Blazquez-Sanchez, A. Austerschulte, A. Voss, T. Graf, and A. Killi, "Improving the brightness of a multi-kW thin disk laser with a single disk by an aspherical phase-front correction," Solid State Lasers Amplifiers IV High-Power Lasers **7721**, 1–8 (2010).

39. A. D. Iebold, F. S. Altarelli, I. J. G. Raumann, C. J. S. Araceno, C. R. P. Hillips, U. K. Eller, A. Diebold, F. Saltarelli, I. J. Graumann, C. J. Saraceno, C. R. Phillips, and U. Keller, "Gas-lens effect in kW-class thin-disk lasers," Opt. Express **26**(10), 12648–12659 (2018).

40. T. Dietrich, C. Röcker, T. Graf, and M. Abdou Ahmed, "Modelling of natural convection in thin-disk lasers," Appl. Phys. B Lasers Opt. **126**(3), 47 (2020).

41. J.-P. Negel, A. Loescher, A. Voss, D. Bauer, D. Sutter, A. Killi, M. Abdou Ahmed, and T. Graf, "Ultrafast thin-disk multipass laser amplifier delivering 1.4 kW (4.7 mJ, 1030 nm) average power converted to 820 W at 515 nm and 234 W at 343 nm," Opt. Express **23**(16), 21064–21077 (2015).

42. R. Paschotta, "Self-phase modulation, explained by RP Photonics Encyclopedia; SPM, Kerr effect, carrier density," https://www.rp-photonics.com/self_phase_modulation.html.

43. P. Kabaciński, T. M. Kardaś, Y. Stepanenko, and C. Radzewicz, "Nonlinear refractive index measurement by SPM-induced phase regression," Opt. Express **27**(8), 11018–11028 (2019).

44. J. Koerner, C. Vorholt, H. Liebetrau, M. Kahle, D. Kloepfel, R. Seifert, J. Hein, and M. C. Kaluza, "Measurement of temperature-dependent absorption and emission spectra of Yb:YAG, Yb:LuAG, and Yb:CaF_2 between 20 °C and 200 °C and predictions on their influence on laser performance," J. Opt. Soc. Am. B **29**(9), 2493–2502 (2012).

45. A. E. Siegman, "Analysis of laser beam quality degradation caused by quartic phase aberrations," Appl. Opt. **32**(30), 5893–5901 (1993).

46. A. E. Siegman and J. Ruff, "Effects of spherical aberration on laser beam quality," in *Laser Energy Distribution Profiles: Measurement and Applications* (SPIE, 1993), Vol. 1834, pp. 130–139.

47. B. R. Suydam, "Effect of Refractive-Index Nonlinearity on the Optical Quality of High-Power Laser Beams," IEEE J. Quantum Electron. **11**(6), 225–230 (1975).

48. W. W. Simmons, J. T. Hunt, and W. E. Warren, "Light Propagation Through Large Laser Systems," IEEE J. Quantum Electron. **17**(9), 1727–1744 (1981).

49. T. Brabec and F. Krausz, "Intense few-cycle laser fields: Frontiers of nonlinear optics," Rev. Mod. Phys. **72**(2), 545–591 (2000).